Anti-wetting and anti-fouling performances of different lubricant-infused slippery surfaces

Yunyi Cao[†], Saikat Jana[†], Xiaolong Tan[ℓ], Leon Bowen[‡], Yufeng Zhu[†], Jack Dawson[†], Rui Han[†], John Exton[†], Hongzhong Liu[§], Glen McHale[‖,#], Nicholas S. Jakubovics[⸸] and Jinju Chen[†]*

[†] School of Engineering, Newcastle University, Newcastle Upon Tyne, NE1 7RU, UK; [ℓ] School of Pharmacy, Newcastle University, Newcastle Upon Tyne, NE1 7RU, UK; [‡] Department of Physics, Durham University, Durham, DH1 3LE, UK;[§] School of Mechanical Engineering, Xi'an Jiaotong University, Xi'an 710054; [‖]Smart Materials and Surfaces Laboratory, Faculty of Engineering and Environment, Northumbria University, Newcastle upon Tyne, NE1 8ST, UK; [#]School of Engineering, University of Edinburgh, Edinburgh, EH9 3FB, UK. [⸸]School of Dental Sciences, Newcastle University, Newcastle Upon Tyne, NE2 4BW, UK.

ABSTRACT

The concept of slippery lubricant-infused surfaces has shown promising potential in anti-fouling for controlling detrimental biofilm growth. In this study, non-toxic silicone oil was either impregnated into porous surface nanostructures, referred as liquid infused surface (LIS), or diffused into a polydimethylsiloxane (PDMS) matrix, referred to as a swollen PDMS (S-PDMS), making two kinds of slippery surfaces. The slippery lubricant layers have extremely low contact angle hysteresis and both slippery surfaces showed superior anti-wetting performances with droplets bouncing off or rolling transiently after impacting the surfaces. We further demonstrated that water droplets can remove dust from the slippery surfaces thus showing a "cleaning effect". Moreover, "coffee-ring" effects were inhibited on these slippery surfaces after droplet evaporation, and deposits could be easily removed. The clinically biofilm-forming species *P. aeruginosa* (as a model system) was used to further evaluate the

antifouling potential of the slippery surfaces. The dried biofilm stains could still be easily removed from the slippery surfaces. Additionally, both slippery surfaces prevented around 90% of bacterial biofilm growth after 6 days, compared to the unmodified control PDMS surfaces. This investigation also extended across another clinical pathogen, *S. epidermidis*, and showed similar results. The anti-wetting and anti-fouling analysis in this study will facilitate the development of more efficient slippery platforms for controlling biofouling.

INTRODUCTION

A biofilm is a sessile community of bacteria in a matrix of extracellular polymeric substances (EPS), which strongly colonizes artificial surfaces when exposed to bulk fluid environments[1]. Biofouling caused by biofilms poses risks and has detrimental consequences for many diverse industries, including potable water treatment and transport, maritime shipping, aquaculture, food processing and biomedical devices[1-2]. Methods to combat biofilm growth on surfaces have included bio-inspired surface textures[3-8], surface grafting with poly(ethylene glycol) (PEG) or zwitterionic polymers[9-10], immobilization of antimicrobial agents[11] (i.e. antibiotics, peptide, silver particles or nitric oxide) and biofilm-dispersing enzymes[12]. For example, superhydrophobic surfaces with high aspect ratio roughness can trap air within micro- or nanostructures, thereby restricting the direct contact between the solid surfaces and micro-organisms[13-15]. The anti-fouling efficacy strongly depends on the lifetime of the non-wetting (Cassie) state, but the wetting transition (Cassie to Wenzel state) can occur within 1-4 hours in submerged environments[13, 16-17]. After that, surface structure can play a key role in biofilm growth, such as isolation effects for delaying cell-cell communications, which has been well demonstrated in our previous work[17]. However, these methods are not sustainable and can only control biofilm growth in the short-term, becoming subsequently overcome by the complex, dynamic, living bacterial system over time[8, 12]. It has been shown that bacteria can adapt and evolve with environments, by either altering gene expression to trigger biofilm formation, or communicating with surrounding bacteria to initiate coordinated activity[12]. Of particular concern, some bacteria (e.g. *Staphylococcus aureus*, *Escherichia coli* and *Pseudomonas aeruginosa*) have evolved into antibiotic-resistant "super-bugs" in order to thrive[3, 12]. Furthermore, the EPS matrix protects biofilms from predators and mediates recalcitrance against biocides, disinfectants, antibiotics, making biofilm removal difficult[1, 11]. The most effective strategy to inhibit or eliminate mature biofilms in the long-term remains an open question and presents a grand challenge.

Inspired by Nepenthes pitcher plants, Aizenberg's group introduced 'slippery liquid-infused porous surface(s)' (SLIPS)[18] to combat long-term biofouling[12, 18-23]. Thus far, there have been at least two different methods (2D versus 3D lubricant infusion), to design stable lubricant-infused surfaces[19, 24]. The first method involves the 2D impregnation of lubricant into the micro/nano-structures with appropriate surface energy, which facilitates the lubricant spreading and retention/blocking via van der Waals and capillary forces to form a stable immiscible over-layer[18-20, 25]. The second method involves the 3D encapsulation and adsorption of lubricant within the cross-linked polymer networks, forming an organogel-like surface[19, 21, 25-27]. Though the initial surface morphology and chemistry of either 2D or 3D slippery surface substrate may be different, a smooth, continuous and homogeneous overlying liquid can form atop these surfaces after the infusion of lubricant[18, 24, 28]. These surfaces restrict direct contact with liquid droplets, which are immiscible with and remain atop the lubricant over-layer[19, 24]. The water droplet on the lubricant moves easily with an extremely low contact angle hysteresis (<5°) [18, 29-30]. Therefore, either 2D or 3D slippery lubricant-infused surfaces can exhibit self-cleaning properties as the droplet can easily remove the surface contamination. Recent studies also demonstrated that slippery surfaces showed exceptional biofouling-repellence against *P. aeruginosa*, *S. aureus*, and *E. coli* biofilm-forming strains, due to the weak bacterial adhesion on the lubricant-liquid interfaces[20-21, 26]. Also, slippery lubricant-infused surfaces have advantages in self-healing, withstanding high external pressure, anti-icing, water harvesting, and thermal management, and show promising potential for industrial applications[31-32].

However, there is a lack of comparison between 2D and 3D slippery lubricant-infused surface and several questions remain elusive. For example, it is not clear whether there are differences in droplet dynamics on these surfaces. Droplets with contaminates coming from rain, dews, or other bulk fluids can cause fouling if pinned on surfaces, due to drying and leaving behind patterned stains[25, 33-34]. Therefore, understanding droplet dynamics on the lubricant layer is critical for us to evaluate their antifouling performance in service.

In the present study, we fabricated 2D and 3D lubricant-infused surfaces as model slippery surfaces: (1) 2D liquid-infused surface (LIS) (often referred as lubricant-impregnated surfaces) after the retention/blocking of silicone oil within the porous epoxy nano-pillars, and (2) 3D swollen polydimethylsiloxane (referred as S-PDMS) after the diffusion of the same lubricant into the polymer network. In other words, the PDMS is swelling owing to the diffusion of silicone oil into the cross-linked matrix[19, 21, 25-27]. The anti-wetting performances of both slippery surfaces were evaluated by considering droplet impact and droplet mobility dynamics.

On the other hand, the anti-fouling performances of slippery surfaces were initially tested against particle dust and dried stains. The typical biofilm-forming strain *P. aeruginosa* was further utilized as a model for the evaluation of anti-biofouling performances. The anti-wetting and anti-fouling performances of the LIS, S-PDMS and the unmodified PDMS (as control) surfaces were systematically compared. These analyses will be invaluable for designing smarter or more efficient anti-fouling surfaces, especially where there is a need to control detrimental biofilm growth.

MATERIALS AND METHODS

Fabrication of slippery surfaces: For the preparation of LIS, the epoxy nano-pillar arrays were made from silicon masters (1×1cm^2 and ~1mm thick) as detailed in the references[8, 16, 35-37]. In this study, the silicon nano-pillar arrays (diameter ~1 μm, space ~2 μm and height~ 2 μm) were fabricated *via* e-beam lithography and were treated with an anti-sticking agent (tridecafluoro-1, 1, 2, 2-tetrahydrooctyl)-trichlorosilane (Gelest Inc.) by exposure in a desiccator under vacuum for 30 minutes. To obtain negative replicas from the silicon substrates, a mixture of PDMS solution was prepared using SYLGARD 184 Elastomer Kit (Dow Corning Corporation, Midland, MI) with a base-to-curing agent ratio of 10:1 (wt/wt). The pre-polymer solution was thoroughly mixed and degassed under vacuum for 30 minutes to eliminate air bubbles. The mixture was poured over the silicon substrates in a Petri dish and cured at 70°C for 2 hours. UV-curable epoxy (OG 142-87, Epoxy Technology, Inc.) was used to get the final imprints of pillars. The epoxy was cured under a UV-lamp, with luminous intensity of 100 mW/cm^2 and wavelength of 365 nm, for 20–25 minutes until fully cured. The epoxy-pillars were checked under the microscope to ensure there was no collapse of pillars before use. Finally, the epoxy-pillars were further treated to increase hydrophobicity using 0.2 mL (tridecafluoro-1, 1, 2, 2-tetrahydrooctyl)-trichlorosilane (Gelest Inc.) by exposure in a desiccator under vacuum overnight.

For the preparation of S-PDMS, a mixture of Poly (dimethylsiloxane) (PDMS) and its curing agent was prepared from SYLGARD 184 Elastomer Kit (Dow Corning Corporation, Midland, MI) with a ratio of 10:1 (wt/wt). The solution was thoroughly mixed and degassed in a vacuum chamber for 30 minutes to eliminate air bubbles. After that, around 14.4 ml of the mixture was poured into a 120 mm square petri dish (Gosselin™), forming around a 1 mm-thickness PDMS

layer. The PDMS was cured at the room temperature for 2 days. Finally, we gently cut the cured PDMS sheet into small pieces (1×1 cm^2).

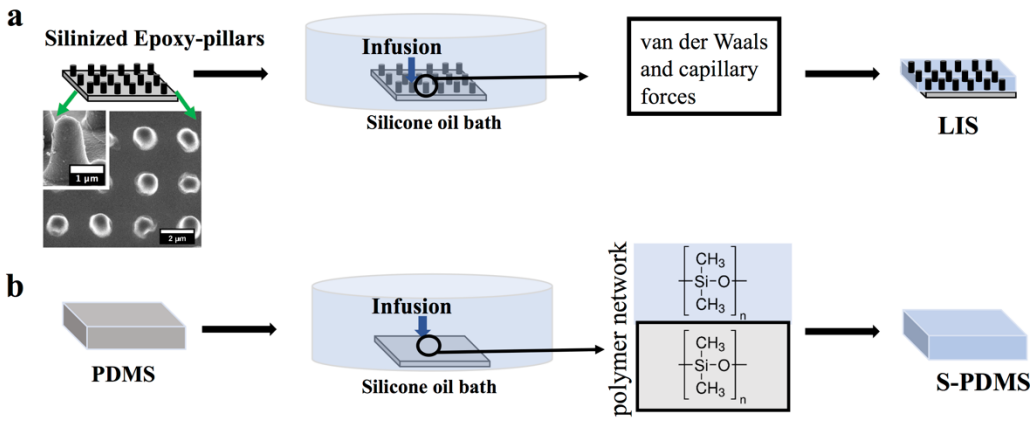

Figure 1. Schematic of the process to make either LIS or S-PDMS slippery surfaces. The SEM image in (a) shows representative surface features (diameter ~1 µm, space ~2 µm and height~ 2 µm) of epoxy-pillars used in this study.

For the infusion of lubricant, either silanized epoxy-pillars or cured PDMS surfaces were completely immersed in a silicone oil (10 cSt, 0.93 g/mL, Sigma-Aldrich) bath and left for 24 hours to allow the lubricant to fully infiltrate into the porous structures of epoxy-pillars or the PDMS polymer networks (Figure 1). The excess lubricant was gently removed from the surface by filter papers, to eliminate the effects of excess lubricant-layer (i.e. wetting ridge[38-41]) on the following tests.

Characterization of slippery surfaces: The epoxy-pillars were imaged by scanning electron microscopy (SEM) using an FEI Helios NanoLab 600 DualBeam system, operated at 5 KV. By using a milligram-balance (OHAUS analytical balance) with a sensitivity of 0.1 mg, the sample weight before and after lubricant-infusion were measured. For the LIS, the thickness of the surface layer having lubricant was estimated based on the measured weight, wetting area and the lubricant density. For S-PDMS, we need to consider the swelling of PDMS infused with silicone when calculating the thickness of surface oil layer. An in-house goniometer[8, 42-43] was set-up to measure the static water contact angle and contact angle hysteresis under ambient conditions. Advancing angles on slippery surfaces were measured via a syringe-pump system (needle gauge size ~25, water droplet ~10 µl, dispersion rate~ 0.2 ml/minute); receding angles were measured as the liquid was withdrawn via the same method[8]. At least five droplet measurements were taken, and the results were presented as the mean contact angles with

standard deviations. There is about 10μm excess oil on LIS. It is expected that the surface stiffness of LIS is dominated by the oil. Where the S-PDMS has little excess oil layer, thus the surface stiffness can be gel-like. Therefore, atomic force microscope (Nanosurf. Ltd) fitted with a spherical probe (radius=1.75μm) was used to do nanoindentation tests at 60nN. At such load, the viscoelastic effect and adhesion were very limited and thus only the Hertz model was adopted.

Droplet impact tests: 10 μL of deionized water droplets were dispersed via a syringe-pump system (needle gauge size ~25, dispersion rate ~0.2 ml/minute) and used in the following measurements. Droplet impact was recorded by a high-speed camera (Photron FASTCAM Mini UX50) at 2000 fps. For the droplet impact test, the Weber number *We* was controlled by the falling height of the drop dispense, thereby resulting in the impact velocity of U_0 =1 m/s and U_0 =4.5 m/s, corresponding to *We* = 21 and *We* = 422, respectively. Here, the *We* number is defined as $We = \rho_w U_0^2 R_0/\gamma_{wa}$, where ρ_w, U_0, R_0, and γ_{wa} are the water density (≈ 1000 kg/m^3), impact velocity, drop radius, and water−air surface tension (≈ 72.4 mN/m), respectively. For the droplet mobility test, all the surfaces were tilted by 15°; and a lower *We* =2 was chosen to better observe the droplet bounce off.

"Self-cleaning" effect tests: The surface fouling was generated by randomly spreading the ground coffee particles or by the stains after evaporating 3 μl of a stardust aqueous solution (3mg/ml, Waitrose Cooks' Homebaking stardust) on surfaces. The dried stains were visualized by a camera with TV lens (50 mm) mounted with an extension tube (40 mm). Deionized water droplets were dispersed as described above and the washing process was recorded by the high-speed camera at 2000 fps.

Bacteria culture and biofouling tests:

Bacteria culture, bacterial adhesion and biofilm growth: Biofilm-forming strain *P. aeruginosa* PAO1-mCherry (Nottingham subline[8, 44]) was used in this study and was routinely cultured in Tryptic Soy Broth (TSB, Melford Laboratories Ltd, UK), in a shaker at 180 rpm, 37℃ for 16 hours prior to the assay of bacterial adhesion/biofilm formation. *P. aeruginosa* PAO1-mCherry was further diluted to OD_{600}= 0.30 with a spectrophotometer (Biochrom Libra S11, Biochrom Ltd., Cambridge, UK). 3 ml of the diluted bacterial culture was incubated with the PDMS (as control), LIS and S-PDMS surfaces in 12-well culture plates at 37℃, for 2 hours (bacterial adhesion assay), 2 days and 6 days (biofilm assay) respectively. For the biofilms developed up

to 6 days, half of the TSB medium was changed every 2 days. At the least three independent experiments were performed for each surface type.

Fluorescent Microscope Analysis: The surfaces after either bacterial adhesion or biofilm formation assay, were gently rinsed three times with Phosphate Buffered Saline (PBS, pH=7.4) to remove loosely adhered bacteria. After that, samples were directly visualized by Olympus BX61 upright fluorescent microscope with a 20x objective lens. The bacterial cells after 2 hours' incubation were visualized by acquiring 2D fluorescent images in a single focal plane (121.25 × 108.75 μm^2). For biofilms, z-stacks were performed through the thickness of biofilm from 5 random locations on the surfaces. The biomass under each field of view (430.00 × 324.38 μm^2) was determined using the COMSTAT2 plugin (Lyngby, Denmark) in ImageJ.

Toxicity Tests: Shaken cultures of *P. aeruginosa* (OD_{600}=0.01) in 20 mL TSB were grown with and without the silicone oil (10% by volume) as described elsewhere[20-21]. Then the bacterial cultures were further incubated in a shaker at 37 °C at 180 rpm. Optical density measurements at 600 nm were taken at 3, 6, and 24 hours with the spectrometer.

Statistical Analysis: Data are represented as mean values with standard error. Student's t-test assuming unequal variations was applied and $*p < 0.05$ was considered statistically significant in this study.

RESULTS AND DISCUSSION

Surface characterisation of different lubricant-infused slippery surfaces

The main criteria to fabricate the LIS surfaces is that the surface is preferentially wetted by the lubricant, while the liquid to be repelled remains atop of the lubricant layer instead of displacing or penetrating it[18]. In order to assess this, it has been proposed that a stable lubricant layer needs to satisfy the following equations[18, 30]:

$$\Delta E_1 = r(\gamma_{oil}\cos\theta_{oil} - \gamma_{water}\cos\theta_{water}) - \gamma_{ow} > 0 \qquad (1)$$

$$\Delta E_2 = r(\gamma_{oil}\cos\theta_{oil} - \gamma_{water}\cos\theta_{water}) + \gamma_{water} - \gamma_{oil} > 0 \qquad (2)$$

where r is the roughness factor (the ratio between the actual and projected surface areas of the textured solid surface); γ_{oil} and γ_{water} are the surface tension of the infused lubricant oil and the water at the air phase, γ_{ow} is the interfacial tension of the oil-water interface; θ_{water} and θ_{oil} are their corresponding contact angles (CA) on the solid surface (with air around) (See detailed

calculation in the Supporting Information). Herein, we generated the ordered pillars (diameter ~1 μm, space ~2 μm and height ~2 μm, see inset SEM image, Figure 1a) on surfaces to provide rough textures for the immobilization of lubricant. After rendering hydrophobic via silanization, we confirmed that our LIS can have a stable lubricant layer (ΔE_1= 31.99 mN/m, ΔE_2=130.99 mN/m). In this study, the initial sample size of LIS and S-PDMS is 1×1 cm^2 and ~1mm thick, thereby the surface volume for lubricant infusion is the same for either surface. We checked the weight difference of samples before and after lubricant infusion with a milligram-balance and found that the lubricant can fully infuse into either surface after 24 hours, as the sample weight did not increase after that time. The infused lubricant on LIS was weighed to be 1.13 ±0.21 mg, and the thickness of the surface layer having lubricant was estimated to be 12.2 ± 2.2 μm. LIS strongly depends on the surface texture for the immobilization of lubricant and generates a thin lubricant oil layer over the texture (i.e. 2 μm height for epoxy-pillars). However, each PDMS sample adsorbed 79.73 ±2.55 mg, nearly 80 times more than LIS and the oil diffuses into the entire PDMS matrix. The S-PDMS was larger in volume than the as-prepared PDMS (see Table 1) because of the swelling[45-46]. The refractive index of the silicone oil and PDMS are almost identical, which makes optical measurements using microscopes difficult. We therefore used a different approach to measure the oil thickness based on the weight difference of swollen PDMS and swollen PDMS with surface oil layer (see Supplement). This gave the oil thickness of (41.1+/-15.2) μm for the S-PDMS, which is thicker than the surface oil of LIS. The atomic force microscope (AFM) nano-indentation measurements (~60 tests) yielded Young's moduli of 719±912 kPa for PDMS, which were comparable to other AFM measurements of this type of PDMS[47] but smaller due to surface effects with small probes at low penetration. The Young's moduli for S-PDMS were 107±94 kPa.

It is also interesting to point out that the stiffness of S-PDMS dropped to about 15% of the PDMS as characterised by atomic force measurements. This suggests the PDMS is capable of strongly locking the oil inside the polymer matrix and behaves like a solid-oil composite. Furthermore, the absorbed oil tends to smooth the PDMS surface which leads to a significantly reduced variation in measured modulus.

Table 1. The key surface features of the surfaces used in this study.

	Substrate volume (area ×thickness)	**Sub-feature dimension**	**Infused lubricant weight(mg)**	**Static contact angle (deg)**	**Contact angle hysteresis (deg)**
PDMS (control)	1cm^2×1mm	n.a.[a]	n.a.[a]	113.0 ± 3.2°	45.2± 4.8°

LIS	1cm^2×1mm	Pillars (diameter~1 µm, pitch~2 µm, height~ 2 µm)	1.13 ±0.21	110.7 ± 5.1°	5.5± 2.7°
S-PDMS	1.21cm^2×1.1mm	n.a.[a]	79.73 ±2.55	104.5 ± 4.9°	3.3± 2.1°

[a]N.a., not applicable.

The static contact angle (CA), and the contact angle hysteresis (CAH) of water droplets on the control PDMS, LIS and S-PDMS were investigated, as summarized in Table 1. LIS has a CA of 110.7 ± 5.1° and S-PDMS has a CA of 104.5 ± 4.9°, which are consistent with the previous experimental investigations[18, 26, 30]. Furthermore, using the spreading coefficient for oil on the liquid droplet in the presence of vapor[30, 41], $S_{ow(a)}= \gamma_{water} - \gamma_{ow} - \gamma_{oil}$, we have demonstrated that $S_{ow(a)} \approx 5.6$ mN/ m. Thus, the silicone oil used in this study may cloak the droplet as $S_{ow(a)} >0$. Therefore, the apparent contact angle θ_{app} can be estimated by the following equation [41, 48]:

$$\cos\theta_{app} = (\gamma_{oil} - \gamma_{ow})/(\gamma_{ow} + \gamma_{oil}) \qquad (3)$$

Equation (3) predicts θ_{app} =108.4°, which is consistent with the CA of LIS within the error estimate. In contrast to the lubricant infused surfaces, the control PDMS without lubricant showed much higher CAH (45.2± 4.8°). However, LIS and S-PDMS have a CAH of 5.5± 2.7° and CAH of 3.3± 2.1°, which are comparable to similar surfaces reported elsewhere[26, 29].

Droplet dynamics on slippery surface

First, we tested if our surfaces can repel water droplets upon impact. Anti-wetting surfaces are required to have a reliable performance against falling droplets, for example rain and dew drops in nature. Herein, we did the drop impact tests at different Weber number (We~ 21 and 422) with the same water droplet volume (10 µl), via fast-imaging analysis. A series of time-resolved images of spreading and retraction dynamics of droplets on the control PDMS, LIS and S-PDMS surfaces were shown in Figure 2 a-b. At either low or high Weber number, there was no noticeable difference during the water drop spreading (0~3.5 ms) among the surfaces. The droplets all deformed into a pancake shape on all surfaces, reaching the maximum diameter (R_{max}) upon impacting after 3.5 ms, which is independent of Weber numbers as previously investigated[49]. We quantitatively examined the ratio R/R_0 of the impacting water drop diameter (R) with respect to the initial drop diameter (R_0) at the different Weber numbers, as shown in Figure 2b. For each case, the plots of R/R_0 against time of different surfaces were nearly collapsing onto a single curve during the spreading, while R_{max}/R_0 increases with the Weber number, indicating that a higher impact velocity results in a fast spreading as the impact time

is the same (3.5 ms). During the droplet retraction at both Weber numbers, the R/R_0 of either LIS or S-PDMS decreased quickly as compared with the control surfaces (Figure 2c), indicating that water droplet is easy to recede on slippery surfaces resulted from their higher receding angles. For either slippery surface, the CAH is very low, thereby the energy dissipation during spreading and receding is low[49]. Therefore, after receding, the drop still has sufficient energy to fully bounce off at a higher Weber number (Figure 2b), which is not the case on the control PDMS having a high CAH. Compared to LIS, even at low Weber number, the droplet on S-PDMS can also partially rebound with a tiny water residual remaining on the surface (Figure 2a). This may suggest further reduced damping and pinning for the droplet atop S-PDMS during spreading and retraction due to further reduced CAH compared to LIS (see Table 1).

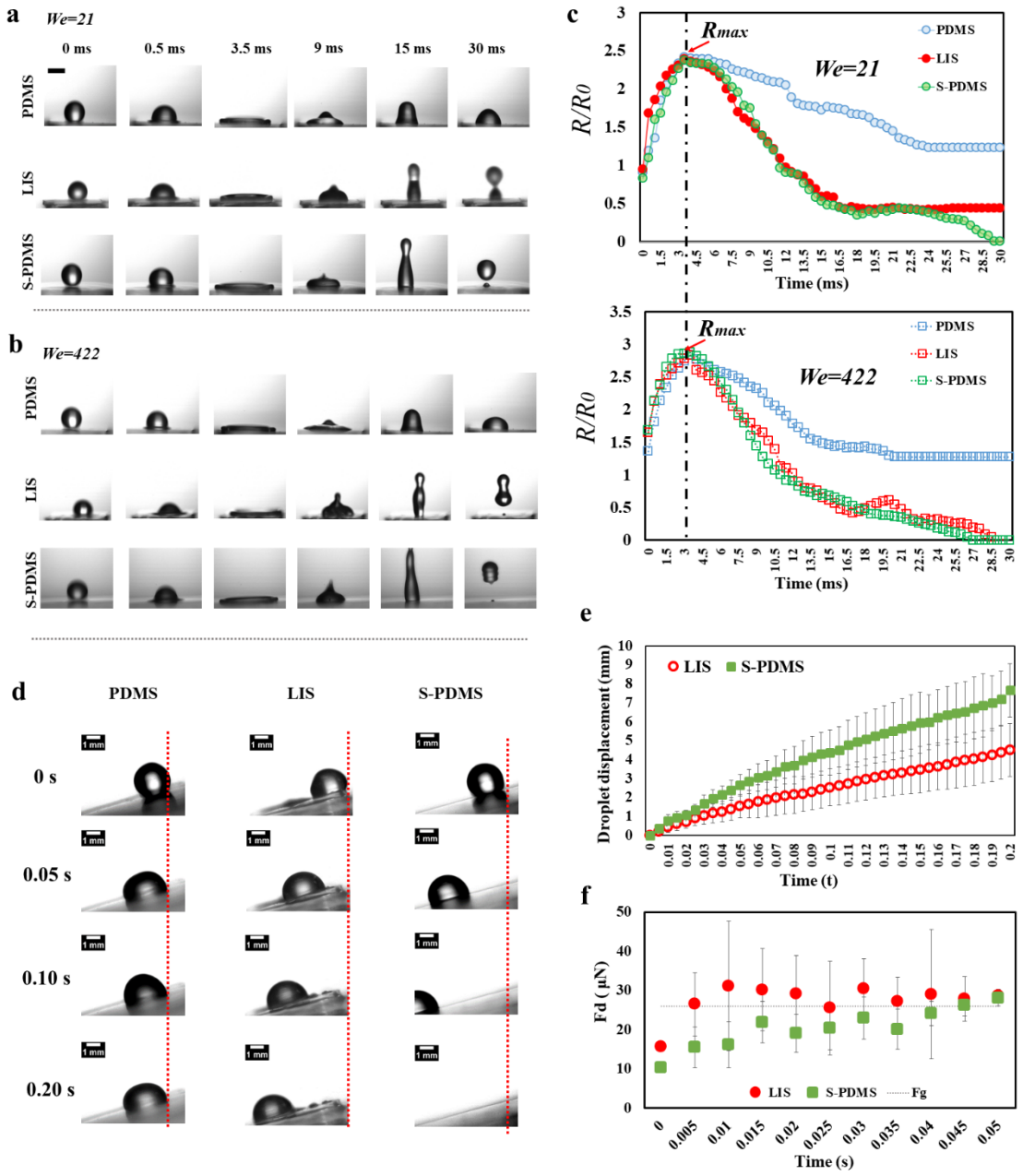

Figure 2. (a-b): Time evolution of a water drop (~10 µl) impacting different surfaces at an impact velocity of (a)U_0 =1 m/s and (b)U_0 =4.5 m/s, corresponding to Weber numbers of We = 21 and We = 422, respectively. The time scale is the same on both figures. Scale bar is 2 mm. (c): Time evolution of the diameter of the impacting water drop normalized by the initial drop diameter at different Weber numbers of on different surfaces. (d): Time evolution of a water drop (~10 µl) moving on the inclined surfaces (tilt angle ~15°). (e): The droplet contact line displacement with time for LIS and S-PDMS surfaces, the displacement varies linearly with time, indicating the droplet is moving with a nearly constant speed. (f): The calculated dissipative force F_d by using equation (4), when droplets move over the slippery surfaces over time (0~ 0.05s).

Next, we sought to investigate the water-shedding ability on inclined surfaces (tilt angle ~15°), as in practice gravity is a common driving force to facilitate the spontaneous water detachment[50]. Droplets are always pinned on the control PDMS surface, corresponding to its high CAH (Figure 2d). However, droplets can be shed from either LIS or S-PDMS surfaces within seconds, showing their superior slippery properties (Figure 2d). Notably, droplets can be shed from the S-PDMS surface within 0.2 s, quicker than the one moving on the LIS surface. To account for this, we quantified the droplet contact line displacement with time for LIS and S-PDMS surfaces as shown in Figure 2e. The droplet moved at a velocity U~ 20.6 ±4.9 mm/s on LIS surface, similar to the value as previously investigated[29]. By contrast, the droplet velocity on S-PDMS is U ~ 36.1±7.1 mm/s, which is significantly quicker and nearly twice of the droplet speed on LIS ($p<0.05$). This may indicate that S-PDMS has a more effective water-shedding ability.

When a droplet is placed on an inclined surface, the mobility of droplets is governed by the gravitational forces ($F_g = mg \sin\theta_{tilt}$) and dissipative forces. F_g was calculated to be about 25.9 μN for control PDMS, LIS and S-PDMS. Here, the dissipative force (F_d) is given by

$$F_d = k \times 2R_b\gamma_{water}(\cos\theta_{Rear} - \cos\theta_{Front}) \qquad (4)$$

where m, g and θ_{tilt} represent the droplet mass, the gravitational acceleration and the inclined angle respectively, θ_{Rear} and θ_{Front} are the apparent rear and front contact angles of the droplet (see Figure S1), R_b is the droplet base radius and γ_{water} is the water/air surface tension[27, 30, 51]. Here, the dimensionless parameter k is related to the actual shape of the drop, which ranged between $4/\pi$ and $\pi/2$ according to analytical models [52],[53] and numerical simulations[54]. A few recent experimental measurements reported that k can be 1.1-1.48 for various droplet on solid surfaces[51]. Here, we also assume that the initial base shape is circle with k=1, which has been widely adopted for estimating the dissipative forces on slippery surfaces[29, 39, 51].

We measured the dynamic R_b, θ_{Rear} and θ_{Front} when droplets moving over the slippery surfaces and calculated F_d by using equation (4) (Figure 2f). 0~ 0.05s was chosen because the droplet moved out of field of view during the recording process thereafter. The initial $F_{d\,(initial)}$ (t~0 s) of control PDMS was 133.5 ±1.6 μN > F_g (~25.9 μN), thereby the droplets always get pinned on the surface as the gravitational force cannot overcome the dissipative force, as seen in Figure 2d. By contrast, $F_{d\,(initial)}$ (t~0 s) of LIS and S-PDMS were 15.8±1.0 μN and 9.7±0.8 μN, which were only around 7-12% of the control PDMS ($F_{d\ (initial)}$ ~133.5 ±1.6 μN) and significantly lower than F_g (~25.9 μN). If we estimated the droplet driving force (F_{drive}) by using the equation

$F_{drive} = F_g - F_d = ma$, where a is the acceleration of the droplet, then F_{drive} is estimated to be ~10.1±1.0 μN for LIS and 16.2±0.8 μN for S-PDMS. Then apparently S-PDMS can have a higher $a_{initial}$ at this transient state, thereby expect to have a higher speed afterwards if assuming the initial droplet moving speed is the same. However, we noted that F_d of either surface increased over time to eventually reach an equilibrium state, where $F_d \approx F_g$ and $F_{drive} \approx 0$, and LIS can reach this state quicker than S-PDMS (Figure 2f). It has been reported that the dissipative force F_d of a moving droplet on lubricated surfaces is also dependent on the viscous stress $\eta U/h$, and $F_d \propto \eta U/h$, where η is the oil viscosity, U is the droplet moving speed, and h is lubricant film thickness[29, 55]. The stable lubricant layer can prevent pinning thereby giving rise to velocity-dependent, viscous dissipative force[29, 55]. Therefore, F_d can increase with U over time, and finally attain the equilibrium, $F_d \approx F_g$ and $F_{drive} \approx 0$. This possibly explained the droplet moving at a nearly constant speed on slippery surfaces afterwards (Figure 2e). Notably, $F_{d(initial)}$ of S-PDMS is lower than LIS, which leads to a higher U as shown in Figure 2e.

Our investigation above demonstrated that water droplets can bounce off S-PDMS surfaces possessing a lower CAH even at a lower Weber number, and droplets can move quicker on the inclined surface. A large difference between LIS and S-PDMS surfaces is that their construction mechanism is different. S-PDMS can adsorb more lubricant volume within the surface and have a thicker lubricant layer as compared with the LIS surface, which possibly results in its stronger slipperiness. Researchers have shown that the CAH of a water drop on a lubricant-infused surface is lower if more lubricant is absorbed, thereby its dissipative force is lower, which significantly improved its mobility speed[22, 25, 56]. In this study, we investigated the droplet dynamics at the macro-scale. Literature reports of the water-lubricant interfaces suggest there is an effective slip length (micro-or nano-scale) of the lubricant layer for the surface slipperiness[19, 55, 57]. It has been reported that S-PDMS can have a thicker effective slip length as compared with similar LIS surfaces, thereby reflecting its greater slipperiness[19]. Other studies have also demonstrated that different lubricant volumes/thickness can lead to different morphologies of the wetting ridge owing to the existence of air-oil-water interfaces[25, 30, 39, 41]. Therefore, the different size/shape of wetting ridge can affect droplet dynamics significantly[30, 38]. After removing the excessive lubricant on either LIS or S-PDMS, the effects of wetting ridge are expected to be eliminated in this study and we did not observe the apparent wetting ridge when investigating the droplet in transient state. However, further studies will be conducted to investigate the effects of slip length and wetting ridge on droplet dynamics in more detail.

Self-cleaning effects of slippery surfaces

A self-cleaning surface is referred as the one from which contaminants such as dusts or stains can easily be removed by a liquid[25]. The water droplets always become pinned on the control PDMS as investigated above. While for either LIS or S-PDMS having a low CAH, we expected that small water droplets can be easily shed from surfaces and take contaminants with them. Firstly, we confirmed the droplet rolling by adding fine ground coffee particles (3 mg/ml) to the water droplet and used the high-speed camera to track the particle motion relative to the droplet when moving across the slippery surfaces (See Support information, video S1). By using an in-house Matlab code, the particle trajectories were generated and are shown in Figure 3. The trajectories of these coffee particles clearly showed that droplets roll across the surface, showing the anti-fouling potentials in practical applications as gravity is a common driving force for the detachment of contaminated water detachment[50]. Then we spread ground coffee particles on inclined LIS and S-PDMS surfaces (tilt angle~15°), and a 10 µl water droplet can still roll away the coffee particles on either surface (Figure 4a). Notably, as the spreading coffee particles were not uniform on surfaces thereby may cause different pinning points, we do not aim to compare the effectiveness of cleaning in this case. While the investigation above showed that either slippery surface has the ability to roll off the surface dusts by water droplets.

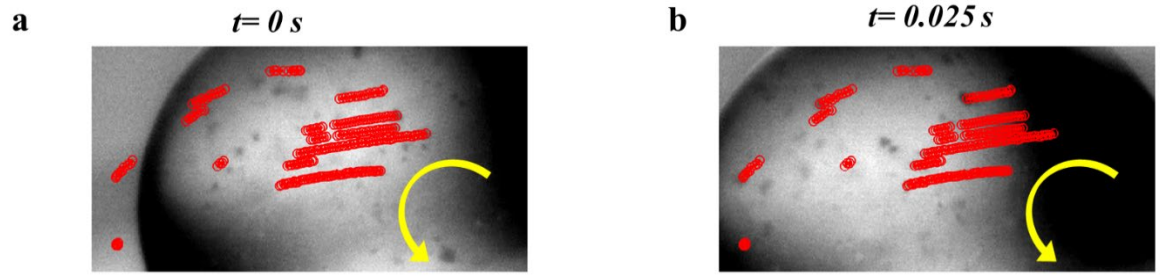

Figure 3. Droplet rolling across the slippery surfaces, captured via fast-imaging camera at 2000 fps. Red circles denote the trajectory of particles as the droplets execute rolling motion between time t=0 to t=0.025 s. Yellow arrows indicate the rolling direction.

Next, we sought to investigate whether slippery surfaces can remove stains easily as the evaporation of contaminated water droplet can leave stains on surfaces (i.e. coffee ring effect), which is difficult to remove[33-34, 50, 58]. The coffee-ring pattern is initiated by the pinning of the droplet three-phase contact line and an evaporation gradient along the droplet surface[34, 59]. Consequently, outward capillary flows inside the drop arise and carry the suspended matter to

the edge of the drop, leading to a ring deposition[33, 50, 58]. The process depends on whether the droplet contact line (CL) is pinned or whether it is able to recede. We investigated this through evaporation of 3 µl of a stardust aqueous solution. The initial CL of droplets were measured to be 1.70 ±0.02 mm for PDMS, 1.85 ±0.07 mm for LIS, and 1.90 ±0.04 mm for S-PDMS, respectively (Figure S2a). The evaporated droplet remained a coffee-ring-like porous dust stain on the PDMS surface in the diameter of 1.68 ±0.06 mm similar to the scale of its initial CL, indicting the CL was mainly pinned and had difficulty in receding (Figure 4b). The stain on LIS was condensed and smaller in the diameter of 1.14 ±0.02 mm (61.6% of its initial CL), implying the CL was more able to recede compared to the PDMS (Figure 4b). The size of the stain on S-PDMS shrank significantly to 0.41 ±0.11 mm (21.6% of its initial CL) and became a lumped deposit, indicating this stain is more condensed and the CL can more easily recede on the S-PDMS surface (Figure 4b). The slight color difference of stains on surfaces (Figure 4b) is possibly owing to the different refractive index at the interfaces (e.g. PDMS-lubricant, or nanostructured epoxy-lubricant). Additionally, we found that the dried stains on either LIS or S-PDMS can be easily removed by tissue papers at once, while the one on the PDMS collapsed into small particles and contaminated the whole surfaces (Figure S2b). The condensed stain on S-PDMS can also be de-pinned and peeled away by a 10 µl water droplet after 0.40 s, in contrast to that a 20 µl water droplet was used for peeling away the stain on LIS after 2.50 s (Figure 4c). The time difference may be attributed to that the stain on LIS is bigger than the one on S-PDMS thereby more energy should be charged to the LIS to release the fresh air-lubricant interface[50]. However, the investigation above demonstrated that the dried dust stains may adsorb to the lubricant layer with easy "peeling-away" via tissue papers or small water droplets, owing to the low adhesion between stain and lubricant interfaces.

It is known that one of the strategies to suppress the coffee ring effect is to prevent the pinning of the contact line. The contact line pinning of a sessile droplet is characterized by the contact angle hysteresis (CAH). Minimizing the hysteresis means suppressing the pinning force per unit length, which facilitates a smoothly receding contact line upon evaporation. This will thus prevent the formation of coffee ring like deposits which was suggested by theoretical models [60-62]. There is accumulated experimental evidence about preventing coffee ring effect when evaporating droplets on low CAH superhydrophobic surfaces[63-65], as observed for slippery surfaces in this study.

The results above indicated the potential of slippery surfaces to inhibit the coffee ring effect owing to the lack of contact line pinning, as found elsewhere[33, 59, 66-67]. However, it has been

reported that the oil wetting ridge may cover part of the droplet rim, thereby hindering the evaporation at the periphery so that the droplet evaporates mainly in the central region of the liquid–air interface. Particles move with the generated upward flow inside the droplet and are captured by the receding liquid–air interface, resulting in uniform deposition[59]. It has also been reported that the diameter of the deposition increased with the increase of either droplet volume or particle concentration[59, 66]. On the other hand, it has been reported that there can be an apparent cloaking effect on micro- or nano-liter droplets on slippery surfaces[27, 68], which is also expected to exist in evaporation process after droplet becomes smaller and which can suppress the evaporation rate. Therefore, the study of the evaporation process with different droplet size/concentration or oil thickness on LIS and S-PDMS is non-trivial but very interesting, and can potentially provide better strategies to prevent coffee-ring effect.

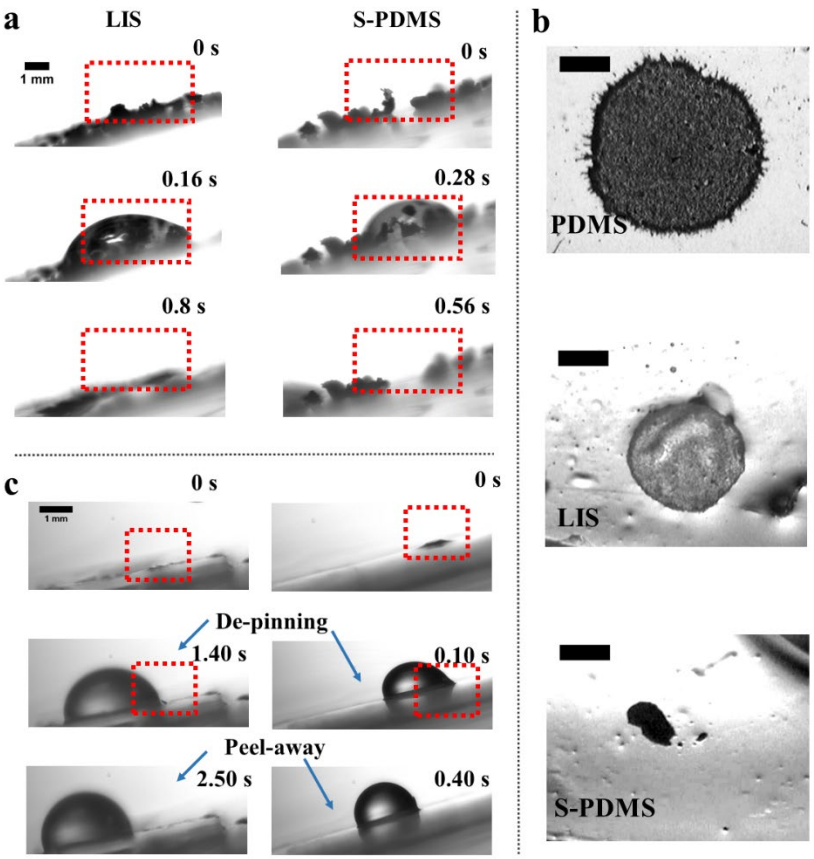

Figure 4. (a): Either LIS or S-PDMS can roll off the spreading coffee particles by water droplets. (b): The residual stains after evaporating 3 µl droplet of a stardust aqueous solution on the surfaces of control PDMS, LIS and S-PDMS, respectively (scale bar 500 µm). (c): The dried dust stains on LIS and S-PDMS can be peeled away by small water droplets.

Anti-biofilm performances of slippery surfaces

Firstly, we investigated the evaporation of 2-days *P. aeruginosa* biofilm culture droplets (Figure 5a and S3a) as well as the dried stains left on the surfaces. Similar to the star dusts investigated above, the evaporated biofilm droplet remained a coffee-ring-like stain on the PDMS surface, similar to the initial CL of biofilm culture droplet (Figure S3 a). Since wiping is often used for cleaning in practical situations, we also used tissue paper as qualitative test to see if they can remove dried biofilm stains. The dried biofilm stain on the PDMS surface was strongly adherent to surface and cannot be wiped or collapsed v*ia* the tissue papers (Figure S3b). However, the biofilm stains on either LIS or S-PDMS were much smaller compared to their initial biofilm droplet CLs (Figure S3a), and either dried biofilm stain can be easily removed by tissue papers with a gentle wipe (Figure S3b and 5a). Also, the biofilm stain on S-PDMS can be peeled away by a 10 µl water droplet after 0.6 s on a surface tilted at 15º (Figure 5b). A 20 µl water droplet cannot peel away the stain on LIS easily with leaving water residues; however, the biofilm stains can still be peeled away after 2-3 times washing with a 20 µl water droplet (Figure S4). The biofilm culture droplets are very viscous and composed of glue-like extracellular polymeric substances (EPS), thereby can strongly adhere onto solid surfaces compared with the aqueous solution. This possibly explained the increased difficulty of de-pinning and peeling biofilm stains from surfaces. However, the investigations above still indicate that slippery surfaces also exhibit anti-fouling characteristics against dried biological contaminant stains such as dehydrated biofilms.

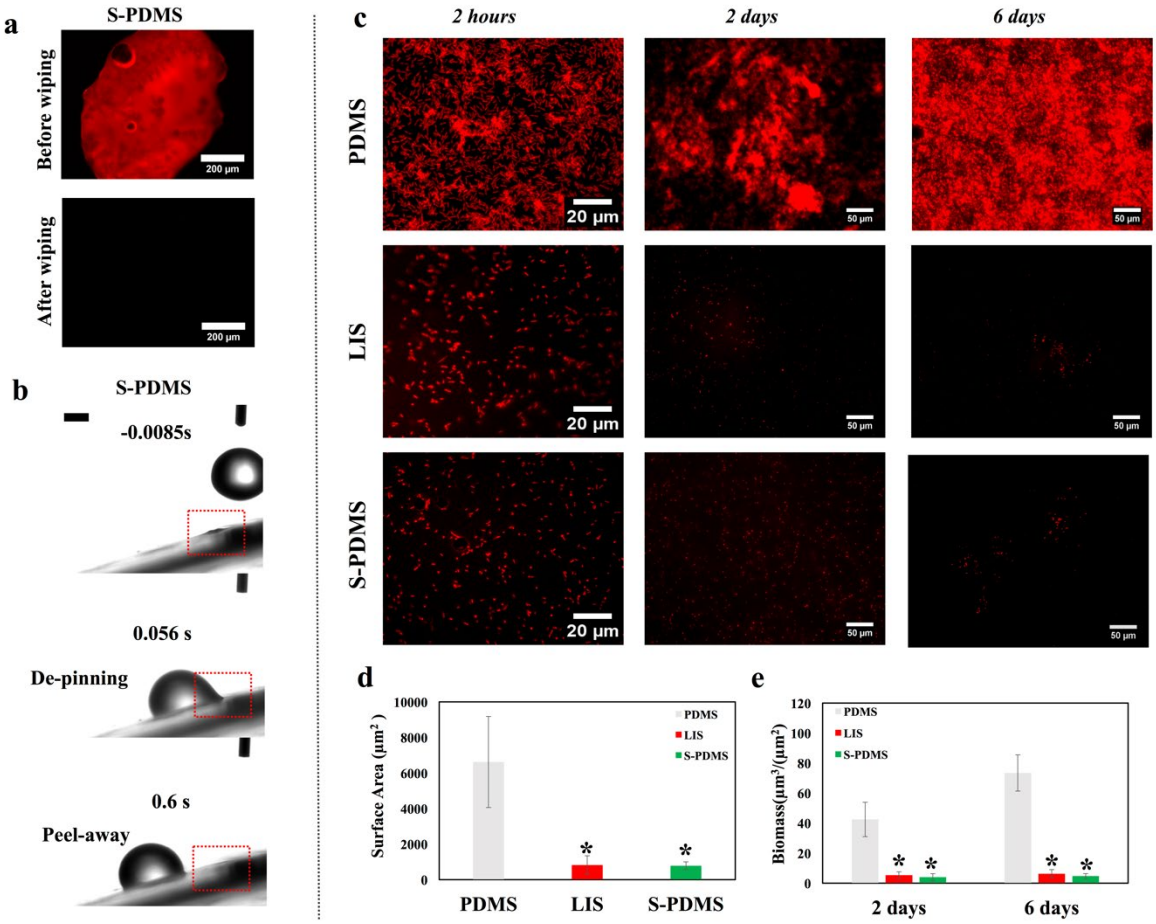

Figure 5. (a): The fluorescent images of dried biofilm stains on S-PDMS showing that they can be easily removed by tissue paper; (b): The biofilm stain on S-PDMS can be peeled away on the surface titled at 15 ° by a 10 μl water droplet after 0.6 s. (c): Fluorescent images of the growth of *P. aeruginosa* at different static cell culture period. (d): The surface area coverage of *P. aeruginosa* in the field of view (121.25 × 108.75 μm^2) for each surface was determined by ImageJ. *$p<0.05$ was considered as significant. (e): Biomass volume per unit area on the different surfaces calculated from ImageJ Comstat2. *$p<0.05$ was considered as significant.

To further evaluate the anti-biofouling properties of slippery surfaces, the growth of *P. aeruginosa* was examined after different timescales (Figure 5c). We firstly examined that if the slippery surface can inhibit the initial bacterial adhesion after 2 hours. As shown in Figure 4c, uniform bacterial attachment was observed on the control PDMS surfaces with locally forming bacterial aggregates or clusters. However, only sparse and isolated cells were seen on either LIS or S-PDMS. Additionally, the quantification of the surface area covered by bacteria (Figure 5d) showed that either LIS or S-PDMS significantly reduced the initial bacterial attachment,

by 85.9 ±10.8% or 86.7 ±5.9% less compared with the control PDMS, respectively. After this, we grew the *P. aeruginosa* biofilms on different surfaces after 2 and 6 days, as shown in the images of maximum intensity projections through the thickness of biofilms (Figure 5c). The control PDMS surfaces showed intense fluorescent patches, indicating a typical biofilm growth comprising multiple layers of cells after 2 and 6 days. *P. aeruginosa* biofilms after 6 days showed a denser and robust biofilm network after the extended culture period with fully covering the surface. In contrast, the slippery surfaces (LIS and S-PDMS) after either 2 days or 6 days, showed no visible adherent biofilms upon being removed from the culture medium, and only had some sparse cells similar to the bacterial attachment after 2 hours (Figure 5c). The total biomass of the LIS and S-PDMS surface after 2 days were significantly lower (86.6 ±7.1% and 90.0 ±6.1% less than the control surface as seen in Figure 5c). Furthermore, we found that the total biomass of the LIS and S-PDMS surface after 6 days were also significantly reduced (91.3 ±3.0% and 93.1 ±3.7 % less than the control surface, as seen in Figure 5e). Notably, there appeared more biofilm reduction on slippery surfaces after 6 days compared with the biofilms after 2 days. The biomass of slippery surfaces measured was 5.3 ±2.7 $\mu m^3/\mu m^2$ of LIS and 4.0 ±2.4 $\mu m^3/\mu m^2$ of S-PDMS after 2 days, 6.3 ±2.7 $\mu m^3/\mu m^2$ of LIS and 4.7 ±1.7 $\mu m^3/\mu m^2$ of S-PDMS after 6 days (Figure 5e). This implied that there was no significant biomass increase during 2-6 days on slippery surfaces, in contrast to the control PDMS where its biofilm biomass after 6 days was nearly twice of the one after 2 days (Figure 5e). Our experimental results were consistent with the previous investigations [20, 23] showing that bacteria have poor ability to anchor a lubricant-liquid “surface” to grow biofilms.

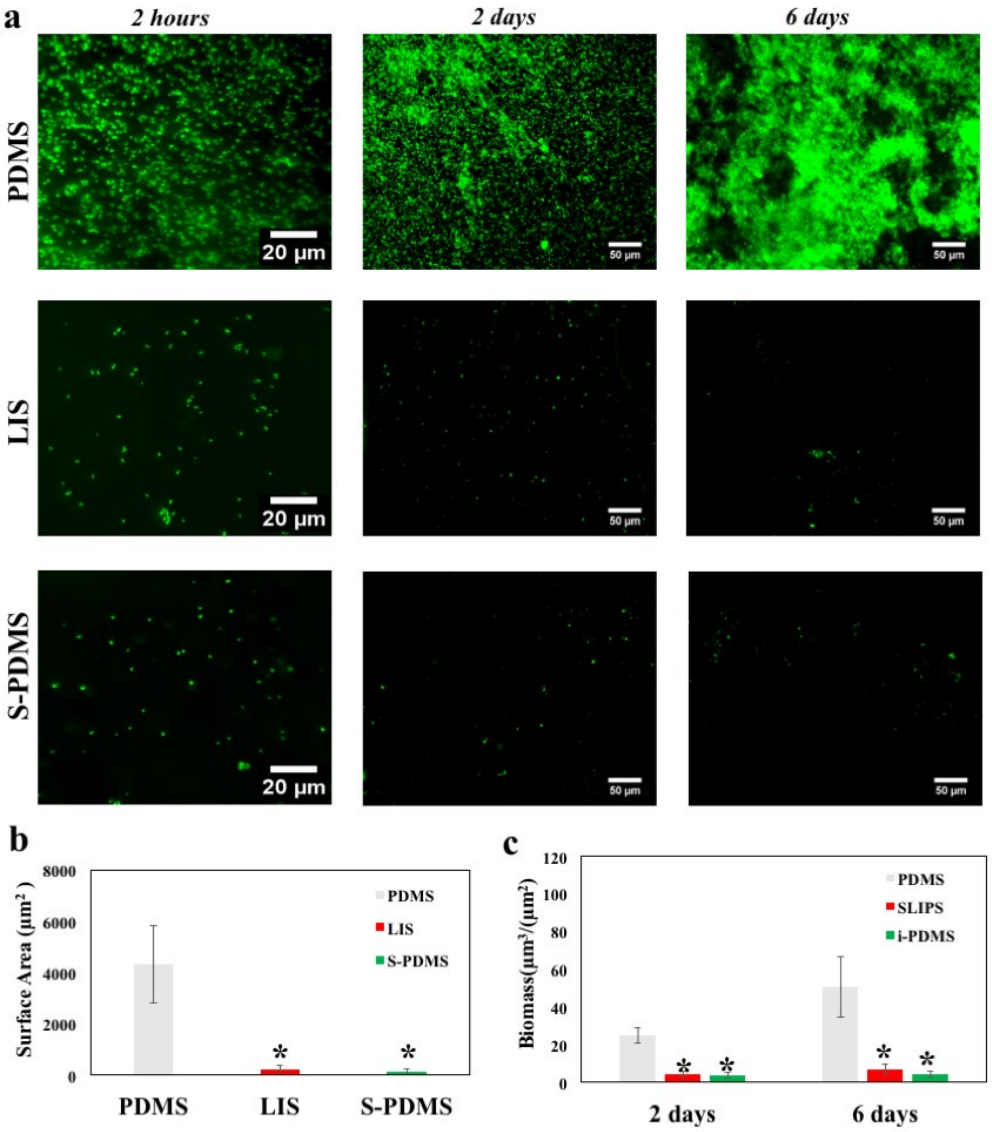

Figure 6. (a): Fluorescent images of the growth of *S. epidermidis* after different timescales. (b): The surface area coverage of *S. epidermidis* in the field of view (121.25 × 108.75 μm^2) for each surface was determined by ImageJ. *$p<0.05$ was considered as significant. (c): Biomass volume per unit area on the different surfaces calculated from ImageJ Comstat2. *$p<0.05$ was considered as significant.

The growth curves of *P. aeruginosa* culture with and without the lubricant (i.e. silicone oil) are shown in Figure S5, and confirmed that the lubricant is nontoxic to the model microorganism used in this study. Silicone oil is non-fluorinated biocompatible liquid and has been widely used in biomedical applications [12]. Therefore, we can confirm that the anti-biofouling performance of our slippery surfaces does not result from the lubricant toxicity, but its special

surface properties. The exceptional ability of our slippery surfaces to resist the biofilm growth of *P. aeruginosa* excited us to find out if they have the potential to inhibit other biofilm growth. We studied the clinically biofilm-forming pathogen, *Staphylococcus epidermidis* (FH-8)[69], for the incubation of 2 hour, 2 days and 6 days (Figure 6). *S. epidermidis* attachment (2 hours) was significantly reduced by 94.4 ±4.9% on LIS and by 95.5 ±3.5% on S-PDMS versus the control PDMS, based on the surface area covered by the adhered bacteria (Figure 6b). The biomass of *S. epidermidis* biofilms (6 days) on the control PDMS was also nearly the twice of the ones after 2 days, showing the continuous biofilm growth (Figure 6c). However, there was also no significant biomass increase of biofilms on slippery surfaces during 2-6 days. *S. epidermidis* biomass of 2 days was significantly reduced by 82.3 ±4.8% on LIS and by 86.1 ±6.6% on S-PDMS versus the control PDMS (Figure 6c). In addition, *S. epidermidis* biomass of the LIS and S-PDMS surface after 6 days were also significantly reduced (85.0 ±8.7% and 90.8 ±3.9 % less), compared with the biomass of the control PDMS surfaces (Figure 6c). This indicated that the anti-biofilm properties of either LIS or S-PDMS is nonspecific and is general to pathogenic biofilm-forming bacteria.

The ease of removing dried biofilm stains and the poor biofilm growth on lubricated slippery surfaces (LIS and S-PDMS) indicate that bacteria interact with slippery surfaces differently from solid surfaces. It has been reported that the lubricant layer on surfaces can impair the mechanical triggers of bacterial biofilm formation [18, 26]. Owing to the smooth slippery properties, bacteria may slide along the lubricant interface with much lower friction-resistance than experienced in the control PDMS [26]. When bacteria are in contact with a smooth lubricant interface, they are not able to anchor to the mobile interface via flagella/pili or other cellular mechanisms as would be possible on a solid surface [20]. This also explained the shrinkage of biofilm stains on slippery surfaces as bacteria cells were sliding/moving along the lubricant with the CL receding. Additionally, the cells still cannot strongly adhere on the lubricant interface after drying, and thereby can be easily removed by tissue papers or small water droplets.

The experimental work above indicated that both slippery surfaces can prevent around 90% of bacterial biofilm growth after 6 days under static conditions, showing similar anti-biofilm properties as stated elsewhere[11, 20-21, 70]. For example, LIS-like slippery surfaces can prevent 99.6% of *P. aeruginosa* biofilm attachment over a 7-d period, as well as *Staphylococcus aureus* (97.2%) and *Escherichia coli* (96%), under both static and flow conditions, as compared with polytetrafluoroethylene (PTFE) surfaces[20]. Similar swollen PDMS slippery surfaces showed 2-

day *S. aureus* biofilm coverages of only 0.1%, compared to 74% and 65% for glass and non-infused PDMS surfaces[21]. Owing to the different material preparation procedure, different bacterial strains used, different experiment conditions (e.g. flow cell or static, culture medium, incubation time), and quantification method also differs, it is challenging to directly compare the anti-biofilm efficacies across different studies. However, together with previous findings[11, 20-21, 70], the results of this study suggested that the anti-biofilm properties of slippery surface are mainly due to the poor adhesion of bacteria at the slippery lubricant interface. However, it was found that Fluoropor-based slippery surfaces with larger porosity cannot effectively inhibit *P. aeruginosa* biofilm growth after 7 days under flow conditions[70]. One possible reason is that the lubricant oil layer is depleted by the orbital flow; and bacterial flagella may aid in the adhesion to infused surfaces although this remains a matter of debate[23]. Here, we didn't observe significant lubricant loss under static culture conditions after 6 days, as no bacterial cells were detected within the lubricant layer. It has also been reported that lubricant loss by cloaking layers can also be minimized by keeping liquid-infused surfaces continuously immersed or formed only smaller wetting ridges[12]. Here we didn't observe significant wetting ridges on either LIS or S-PDMS.

For practical applications, durability is very important for anti-fouling surfaces. We have performed preliminary tests to evaluate if high CA and low CAH may be retained after droplet impact and washing away of biofilms. We have demonstrated that the slippery surfaces still have low CAH after multiple droplet impacts, which suggests good anti-wetting performance is maintained. After washing away 2 day-old biofilms, the CAH is still as low as when the surface was prepared which suggests that it can be reused as an anti-fouling surface. However, it would be useful for future work to consider the effect on lubricant depletion under different practical conditions (e.g. evaporation at elevated temperatures, under different flow conditions) of changing adsorbing lubricant (e.g. volumes or viscosity) within either LIS or S-PDMS.

CONCLUSIONS

In summary, this study evaluated the anti-wetting and anti-fouling performances of the slippery lubricant-infused surfaces by two different model surfaces: LIS and S-PDMS. The stable immiscible lubricant-layer enables these slippery surfaces to repel water droplets compared to the PDMS control surface. S-PDMS showed even smaller contact angle hysteresis (~3.3 °) than LIS (~5.5°) possibly due to thicker lubricant layer on surface and larger amount of oil adsorbed

within the polymer chains of PDMS. The stored oil in S-PDMS can replenish after the surface oil is removed and thus facilitate reusability and a sustainable antifouling/anti-wetting performance. Therefore, S-PDMS tends to outperform LIS in terms of antifouling/anti-wetting performance. The droplet dynamics tests have shown that the water droplet is more likely to bounce back in those slippery surfaces at both low and high Weber numbers, particularly for S-PDMS. This implies the lower energy dissipation of these two slippery surfaces due to lower contact angle hysteresis. Our quantitative analysis has demonstrated that the dissipative forces for the slippery surface are a fraction (7-12%) of the PDMS surface when tilted at 15°. As a result, the difference between the contribution of gravity force and dissipative force makes droplet to shield quickly, and can also roll over the dusts from both slippery surfaces, which makes them self-cleaning surfaces. Particularly, the coffee ring effect is inhibited on slippery surfaces owing to the lack of contact line pinning of droplets, thereby only condensed deposits are formed after the evaporation of dust or biofilm droplets. These stains can be easily removed by tissue wiping or small water droplets.

Additionally, both slippery surfaces exhibited strong anti-fouling characteristics against *P. aeruginosa* and *S. epidermidis* biofilms under static conditions even after 6 days. The construction mechanism of LIS and S-PDMS may also provide insights to guide the fabrication of slippery platforms using different materials. LIS can be created onto a variety of materials where surface textures can be applied, for example, polymers, titanium, steels, and glasses[11, 32, 70-71]. However, the costs of fabricating a large area of surface textures could be very high. The creation of S-PDMS involves a cheap and easy fabrication process which strongly depends on the cross-linked polymer network to absorb the lubricant. Making polymer coatings or sprayable paints may allow for a large-scale application on arbitrary surfaces. This study provides a promising anti-wetting slippery lubricant-infused surfaces for controlling bio-fouling, especially those triggered by biofilm growth. However, we note that the long-term antifouling efficiency and reusability of different slippery surfaces is not well understood. Therefore, it would be useful to study the re-usability of the slippery surfaces in flow conditions. It would also be interesting to study how different bacterial mutants (with/ without flagella or pili) may affect the interactions between bacteria and the lubricant layer.

ASSOCIATED CONTENT

Supporting Information : The Supporting Information is available free of charge on the ACS Publications website at DOI: XXXXX. Method for the measurement of oil thickness for S-

PDMS. Calculations to determine if stable lubricant layer can form on materials surfaces. Schematic for the calculation of dissipative forces. Digital images of contact line of water droplets on different surfaces and dried stardust stains on different surfaces. Digital images of contact line of water droplets on surfaces and the dried biofilm stain on different surfaces. Digital images of washing dried biofilm stain using 20 µl water droplet. Growth curves of P. aeruginosa cultured in shaken TB media containing 1% of silicon oil.

AUTHOR INFORMATION

Corresponding Author

* *Jinju Chen: Email: jinju.chen@ncl.ac.uk*

Author Contributions

All authors contributed to this work. Y.C., S.J., X.T., H.L., G.M., N.J. and J.C. designed the research. Y.C. and S.J. performed drop impact tests and analyzed the data. Y.C. performed most experiments and acquired the data, and did data analysis. L.B. and X.T. conducted the SEM experiments. YZ, JD, RH, JE, JC performed AFM measurements and data analysis. JD, YZ and JC measured the oil thickness of S-PDMS and did measurements and analysis of CA and CAH to demonstrate re-usability of the slippery surfaces. Y.C., GM, N.J. and J.C. prepared the original draft. All authors reviewed and edited the manuscript. All authors have given approval to the final version of the manuscript.

ACKNOWLEDGMENTS

Y. Cao acknowledges the PhD studentship (Research Excellence Academy funding scheme) from Newcastle University. J. Dawson and J. Exton acknowledge the EPSRC DTP scholarships. R. Han acknowledge the PhD scholarship from Chinese Scholarship Council and Newcastle University. J. Chen acknowledges funding from the Engineering and Physical Sciences Research Council (EP/K039083/1, EP/R025606/1) and EPSRC Partnering for GCRF(EP/R512692/1). We also acknowledge the technical assistance and useful discussions with Dr Nadia Rostami, Dr. Kristian Franze, Dr Rebecca Jones, Dr. Ben Allen, Dr. Rolando Berlinguer-Palmini, Ekaterina Kozhevnikova and Bethany Orme.

REFERENCES

(1) Berne, C.; Ellison, C. K.; Ducret, A.; Brun, Y. V. Bacterial adhesion at the single-cell level. *Nature Reviews Microbiology* **2018,** *16*, 616-27.
(2) Molino, P. J.; Yang, D.; Penna, M.; Miyazawa, K.; Knowles, B. R.; MacLaughlin, S.; Fukuma, T.; Yarovsky, I.; Higgins, M. J. Hydration layer structure of biofouling-resistant nanoparticles. *ACS nano* **2018,** *12* (11), 11610-11624.
(3) Cao, Y.; Su, B.; Chinnaraj, S.; Jana, S.; Bowen, L.; Charlton, S.; Duan, P.; Jakubovics, N. S.; Chen, J. Nanostructured titanium surfaces exhibit recalcitrance towards Staphylococcus epidermidis biofilm formation. *Scientific reports* **2018,** *8* (1), 1071.
(4) Diu, T.; Faruqui, N.; Sjostrom, T.; Lamarre, B.; Jenkinson, H. F.; Su, B.; Ryadnov, M. G. Cicada-inspired cell-instructive nanopatterned arrays. *Sci Rep* **2014,** *4*, 7122, DOI: 10.1038/srep07122.
(5) Bhadra, C. M.; Truong, V. K.; Pham, V. T.; Al Kobaisi, M.; Seniutinas, G.; Wang, J. Y.; Juodkazis, S.; Crawford, R. J.; Ivanova, E. P. Antibacterial titanium nano-patterned arrays inspired by dragonfly wings. *Sci Rep* **2015,** *5*, 16817, DOI: 10.1038/srep16817.
(6) Fadeeva, E.; Truong, V. K.; Stiesch, M.; Chichkov, B. N.; Crawford, R. J.; Wang, J.; Ivanova, E. P. Bacterial retention on superhydrophobic titanium surfaces fabricated by femtosecond laser ablation. *Langmuir* **2011,** *27* (6), 3012-3019.
(7) Ivanova, E. P.; Hasan, J.; Webb, H. K.; Truong, V. K.; Watson, G. S.; Watson, J. A.; Baulin, V. A.; Pogodin, S.; Wang, J. Y.; Tobin, M. J.; Lobbe, C.; Crawford, R. J. Natural bactericidal surfaces: mechanical rupture of Pseudomonas aeruginosa cells by cicada wings. *Small* **2012,** *8* (16), 2489-94, DOI: 10.1002/smll.201200528.
(8) Cao, Y.; Jana, S.; Bowen, L.; Tan, X.; Liu, H.; Rostami, N.; Brown, J.; Jakubovics, N. S.; Chen, J. Hierarchical rose-petal surfaces delay the early-stage bacterial biofilm growth. *Langmuir* **2019**.
(9) Cheng, G.; Zhang, Z.; Chen, S.; Bryers, J. D.; Jiang, S. Inhibition of bacterial adhesion and biofilm formation on zwitterionic surfaces. *Biomaterials* **2007,** *28* (29), 4192-4199.
(10) Cheng, G.; Li, G.; Xue, H.; Chen, S.; Bryers, J. D.; Jiang, S. Zwitterionic carboxybetaine polymer surfaces and their resistance to long-term biofilm formation. *Biomaterials* **2009,** *30* (28), 5234-5240.
(11) Li, J.; Kleintschek, T.; Rieder, A.; Cheng, Y.; Baumbach, T.; Obst, U.; Schwartz, T.; Levkin, P. A. Hydrophobic liquid-infused porous polymer surfaces for antibacterial applications. *ACS applied materials & interfaces* **2013,** *5* (14), 6704-6711.
(12) Howell, C.; Grinthal, A.; Sunny, S.; Aizenberg, M.; Aizenberg, J. Designing Liquid - Infused Surfaces for Medical Applications: A Review. *Advanced Materials* **2018,** *30* (50), 1802724.

(13) Truong, V. K.; Webb, H. K.; Fadeeva, E.; Chichkov, B. N.; Wu, A. H. F.; Lamb, R.; Wang, J. Y.; Crawford, R. J.; Ivanova, E. P. Air-directed attachment of coccoid bacteria to the surface of superhydrophobic lotus-like titanium. *Biofouling* **2012,** *28* (6), 539-550.
(14) Tang, P.; Zhang, W.; Wang, Y.; Zhang, B.; Wang, H.; Lin, C.; Zhang, L. Effect of superhydrophobic surface of titanium on staphylococcus aureus adhesion. *Journal of Nanomaterials* **2011,** *2011*, 2.
(15) Ma, J.; Sun, Y.; Gleichauf, K.; Lou, J.; Li, Q. Nanostructure on taro leaves resists fouling by colloids and bacteria under submerged conditions. *Langmuir* **2011,** *27* (16), 10035-10040.
(16) Friedlander, R. S.; Vlamakis, H.; Kim, P.; Khan, M.; Kolter, R.; Aizenberg, J. Bacterial flagella explore microscale hummocks and hollows to increase adhesion. *Proceedings of the National Academy of Sciences* **2013,** *110* (14), 5624-5629.
(17) Cao, Y.; Jana, S.; Bowen, L.; Tan, X.; Liu, H.; Rostami, N.; Brown, J.; Jakubovics, N. S.; Chen, J. Hierarchical Rose Petal Surfaces Delay the Early-Stage Bacterial Biofilm Growth. *Langmuir* **2019,** *35* (45), 14670-14680.
(18) Wong, T.-S.; Kang, S. H.; Tang, S. K.; Smythe, E. J.; Hatton, B. D.; Grinthal, A.; Aizenberg, J. Bioinspired self-repairing slippery surfaces with pressure-stable omniphobicity. *Nature* **2011,** *477* (7365), 443.
(19) Amini, S.; Kolle, S.; Petrone, L.; Ahanotu, O.; Sunny, S.; Sutanto, C. N.; Hoon, S.; Cohen, L.; Weaver, J. C.; Aizenberg, J. Preventing mussel adhesion using lubricant-infused materials. *Science* **2017,** *357* (6352), 668-673.
(20) Epstein, A. K.; Wong, T.-S.; Belisle, R. A.; Boggs, E. M.; Aizenberg, J. Liquid-infused structured surfaces with exceptional anti-biofouling performance. *Proceedings of the National Academy of Sciences* **2012,** *109* (33), 13182-13187.
(21) Howell, C.; Vu, T. L.; Lin, J. J.; Kolle, S.; Juthani, N.; Watson, E.; Weaver, J. C.; Alvarenga, J.; Aizenberg, J. Self-replenishing vascularized fouling-release surfaces. *ACS applied materials & interfaces* **2014,** *6* (15), 13299-13307.
(22) Kim, P.; Kreder, M. J.; Alvarenga, J.; Aizenberg, J. Hierarchical or not? Effect of the length scale and hierarchy of the surface roughness on omniphobicity of lubricant-infused substrates. *Nano letters* **2013,** *13* (4), 1793-1799.
(23) Kovalenko, Y.; Sotiri, I.; Timonen, J. V.; Overton, J. C.; Holmes, G.; Aizenberg, J.; Howell, C. Bacterial interactions with immobilized liquid layers. *Advanced healthcare materials* **2017,** *6* (15), 1600948.
(24) Wei, C.; Zhang, G.; Zhang, Q.; Zhan, X.; Chen, F. Silicone oil-infused slippery surfaces based on Sol–Gel process-induced nanocomposite coatings: A facile approach to highly stable bioinspired surface for biofouling resistance. *ACS applied materials & interfaces* **2016,** *8* (50), 34810-34819.
(25) Solomon, B. R.; Subramanyam, S. B.; Farnham, T. A.; Khalil, K. S.; Anand, S.; Varanasi, K. K. Lubricant-impregnated surfaces. In *Non-wettable Surfaces*; 2016; pp 285-318.

(26) MacCallum, N.; Howell, C.; Kim, P.; Sun, D.; Friedlander, R.; Ranisau, J.; Ahanotu, O.; Lin, J. J.; Vena, A.; Hatton, B. Liquid-infused silicone as a biofouling-free medical material. *ACS Biomaterials Science & Engineering* **2014,** *1* (1), 43-51.
(27) Jiang, J.; Zhang, H.; He, W.; Li, T.; Li, H.; Liu, P.; Liu, M.; Wang, Z.; Wang, Z.; Yao, X. Adhesion of microdroplets on water-repellent surfaces toward the prevention of surface fouling and pathogen spreading by respiratory droplets. *ACS applied materials & interfaces* **2017,** *9* (7), 6599-6608.
(28) Daniel, D.; Timonen, J. V.; Li, R.; Velling, S. J.; Aizenberg, J. Oleoplaning droplets on lubricated surfaces. *Nature Physics* **2017,** *13* (10), 1020-1025.
(29) Daniel, D.; Timonen, J. V.; Li, R.; Velling, S. J.; Kreder, M. J.; Tetreault, A.; Aizenberg, J. Origins of extreme liquid repellency on structured, flat, and lubricated hydrophobic surfaces. *Physical review letters* **2018,** *120* (24), 244503.
(30) Smith, J. D.; Dhiman, R.; Anand, S.; Reza-Garduno, E.; Cohen, R. E.; McKinley, G. H.; Varanasi, K. K. Droplet mobility on lubricant-impregnated surfaces. *Soft Matter* **2013,** *9* (6), 1772-1780.
(31) Lee, C.; Kim, H.; Nam, Y. Drop impact dynamics on oil-infused nanostructured surfaces. *Langmuir* **2014,** *30* (28), 8400-8407.
(32) Wang, P.; Zhang, D.; Sun, S.; Li, T.; Sun, Y. Fabrication of slippery lubricant-infused porous surface with high underwater transparency for the control of marine biofouling. *ACS applied materials & interfaces* **2016,** *9* (1), 972-982.
(33) McBride, S. A.; Dash, S.; Varanasi, K. K. Evaporative crystallization in drops on superhydrophobic and liquid-impregnated surfaces. *Langmuir* **2018,** *34* (41), 12350-12358.
(34) Deegan, R. D.; Bakajin, O.; Dupont, T. F.; Huber, G.; Nagel, S. R.; Witten, T. A. Capillary flow as the cause of ring stains from dried liquid drops. *Nature* **1997,** *389* (6653), 827.
(35) Kim, P.; Adorno-Martinez, W. E.; Khan, M.; Aizenberg, J. Enriching libraries of high-aspect-ratio micro-or nanostructures by rapid, low-cost, benchtop nanofabrication. *nature protocols* **2012,** *7* (2), 311.
(36) Hochbaum, A. I.; Aizenberg, J. Bacteria pattern spontaneously on periodic nanostructure arrays. **2010**.
(37) Pokroy, B.; Epstein, A. K.; Persson-Gulda, M.; Aizenberg, J. Fabrication of bioinspired actuated nanostructures with arbitrary geometry and stiffness. *Advanced Materials* **2009,** *21* (4), 463-469.
(38) Sadullah, M. S.; Semprebon, C.; Kusumaatmaja, H. Drop dynamics on liquid-infused surfaces: The role of the lubricant ridge. *Langmuir* **2018,** *34* (27), 8112-8118.
(39) Semprebon, C.; McHale, G.; Kusumaatmaja, H. Apparent contact angle and contact angle hysteresis on liquid infused surfaces. *Soft matter* **2017,** *13* (1), 101-110.

(40) Schellenberger, F.; Xie, J.; Encinas, N.; Hardy, A.; Klapper, M.; Papadopoulos, P.; Butt, H.-J.; Vollmer, D. Direct observation of drops on slippery lubricant-infused surfaces. *Soft Matter* **2015,** *11* (38), 7617-7626.
(41) McHale, G.; Orme, B. V.; Wells, G. G.; Ledesma-Aguilar, R. Apparent Contact Angles on Lubricant-Impregnated Surfaces/SLIPS: From Superhydrophobicity to Electrowetting. *Langmuir* **2019,** *35* (11), 4197-4204.
(42) Gart, S.; Mates, J. E.; Megaridis, C. M.; Jung, S. Droplet impacting a cantilever: A leaf-raindrop system. *Physical Review Applied* **2015,** *3* (4), 044019.
(43) Huhtamäki, T.; Tian, X.; Korhonen, J. T.; Ras, R. H. Surface-wetting characterization using contact-angle measurements. *Nature protocols* **2018,** *13* (7), 1521.
(44) Sidorenko, J.; Jatsenko, T.; Kivisaar, M. Ongoing evolution of Pseudomonas aeruginosa PAO1 sublines complicates studies of DNA damage repair and tolerance. *Mutation Research/Fundamental and Molecular Mechanisms of Mutagenesis* **2017,** *797*, 26-37.
(45) Zhang, P.; Liu, H.; Meng, J.; Yang, G.; Liu, X.; Wang, S.; Jiang, L. Grooved organogel surfaces towards anisotropic sliding of water droplets. *Advanced Materials* **2014,** *26* (19), 3131-3135.
(46) Yao, X.; Wu, S.; Chen, L.; Ju, J.; Gu, Z.; Liu, M.; Wang, J.; Jiang, L. Self-Replenishable Anti - Waxing Organogel Materials. *Angewandte Chemie International Edition* **2015,** *54* (31), 8975-8979.
(47) Suriano, R.; Credi, C.; Levi, M.; Turri, S. AFM nanoscale indentation in air of polymeric and hybrid materialswith highly different stiffness. *Applied Surface Science* **2014,** *311*, 558–566.
(48) Kreder, M. J.; Daniel, D.; Tetreault, A.; Cao, Z.; Lemaire, B.; Timonen, J. V.; Aizenberg, J. Film dynamics and lubricant depletion by droplets moving on lubricated surfaces. *Physical Review X* **2018,** *8* (3), 031053.
(49) Muschi, M.; Brudieu, B.; Teisseire, J.; Sauret, A. Drop impact dynamics on slippery liquid-infused porous surfaces: influence of oil thickness. *Soft matter* **2018,** *14* (7), 1100-1107.
(50) Cao, M.; Guo, D.; Yu, C.; Li, K.; Liu, M.; Jiang, L. Water-repellent properties of superhydrophobic and lubricant-infused "slippery" surfaces: a brief study on the functions and applications. *ACS applied materials & interfaces* **2015,** *8* (6), 3615-3623.
(51) Gao, N.; Geyer, F.; Pilat, D. W.; Wooh, S.; Vollmer, D.; Butt, H.-J.; Berger, R. How drops start sliding over solid surfaces. *Nature Physics* **2018,** *14* (2), 191.
(52) Extrand, C. W.; Gent, A. N. RETENTION OF LIQUID-DROPS BY SOLID-SURFACES. *Journal of Colloid and Interface Science* **1990,** *138* (2), 431-442, DOI: 10.1016/0021-9797(90)90225-d.
(53) ElSherbini, A.; Jacobi, A. M. Retention forces and contact angles for critical liquid drops on non-horizontal surfaces. *Journal of colloid and interface science* **2006,** *299* (2), 841-849.

(54) Brown, R. A.; Orr, F. M.; Scriven, L. E. STATIC DROP ON AN INCLINED PLATE - ANALYSIS BY THE FINITE-ELEMENT METHOD. *Journal of Colloid and Interface Science* **1980,** *73* (1), 76-87, DOI: 10.1016/0021-9797(80)90124-1.
(55) Daniel, D.; Timonen, J. V. I.; Li, R.; Velling, S. J.; Aizenberg, J. Oleoplaning droplets on lubricated surfaces. *Nature Physics* **2017,** *13* (10), 1020.
(56) Zhang, J.; Wang, A.; Seeger, S. Nepenthes pitcher inspired anti-wetting silicone nanofilaments coatings: preparation, unique anti-wetting and self-cleaning behaviors. *Advanced Functional Materials* **2014,** *24* (8), 1074-1080.
(57) Scarratt, L. R.; Zhu, L.; Neto, C. How Slippery are SLIPS? Measuring Effective Slip on Lubricated Surfaces with Colloidal Probe Atmoc Force Microscopy. *Langmuir* **2019,** *35* (8), 2976-2982.
(58) Yunker, P. J.; Still, T.; Lohr, M. A.; Yodh, A. Suppression of the coffee-ring effect by shape-dependent capillary interactions. *Nature* **2011,** *476* (7360), 308.
(59) Gao, A.; Liu, J.; Ye, L.; Schönecker, C.; Kappl, M.; Butt, H.-J. r.; Steffen, W. Control of Droplet Evaporation on Oil-Coated Surfaces for the Synthesis of Asymmetric Supraparticles. *Langmuir* **2019,** *35* (43), 14042-14048.
(60) Frastia, L.; Archer, A. J.; Thiele, U. Dynamical Model for the Formation of Patterned Deposits at Receding Contact Lines. *Physical Review Letters* **2011,** *106* (7), DOI: 10.1103/PhysRevLett.106.077801.
(61) Freed-Brown, J. Evaporative deposition in receding drops. *Soft Matter* **2014,** *10* (47), 9506-9510, DOI: 10.1039/c4sm02133a.
(62) Man, X. K.; Doi, M. S. Ring to Mountain Transition in Deposition Pattern of Drying Droplets. *Physical Review Letters* **2016,** *116* (6), DOI: 10.1103/PhysRevLett.116.066101.
(63) Cui, L. Y.; Zhang, J. H.; Zhang, X. M.; Li, Y. F.; Wang, Z. H.; Gao, H. N.; Wang, T. Q.; Zhu, S. J.; Yu, H. L.; Yang, B. Avoiding coffee ring structure based on hydrophobic silicon pillar arrays during single-drop evaporation. *Soft Matter* **2012,** *8* (40), 10448-10456, DOI: 10.1039/c2sm26271a.
(64) Brunet, P. Particle deposition after droplet evaporation on ultra-hydrophobic micro-textured surfaces. *Soft Matter* **2012,** *8* (44), 11294-11301, DOI: 10.1039/c2sm26161h.
(65) Dicuangco, M.; Dash, S.; Weibel, J. A.; Garimella, S. V. Effect of superhydrophobic surface morphology on evaporative deposition patterns. *Applied Physics Letters* **2014,** *104* (20), DOI: 10.1063/1.4878322.
(66) Tan, H.; Wooh, S.; Butt, H.-J.; Zhang, X.; Lohse, D. Porous supraparticle assembly through self-lubricating evaporating colloidal ouzo drops. *Nature communications* **2019,** *10* (1), 1-8.
(67) Yang, S.; Dai, X.; Stogin, B. B.; Wong, T.-S. Ultrasensitive surface-enhanced Raman scattering detection in common fluids. *Proceedings of the National Academy of Sciences* **2016,** *113* (2), 268-273.

(68) Pham, Q. N.; Zhang, S.; Montazeri, K.; Won, Y. Droplets on Slippery Lubricant-Infused Porous Surfaces: A Macroscale to Nanoscale Perspective. *Langmuir* **2018,** *34* (47), 14439-14447.
(69) Shields, R. C.; Mokhtar, N.; Ford, M.; Hall, M. J.; Burgess, J. G.; ElBadawey, M. R.; Jakubovics, N. S. Efficacy of a marine bacterial nuclease against biofilm forming microorganisms isolated from chronic rhinosinusitis. *PLoS One* **2013,** *8* (2), e55339.
(70) Keller, N.; Bruchmann, J.; Sollich, T.; Richter, C.; Thelen, R.; Kotz, F.; Schwartz, T.; Helmer, D.; Rapp, B. E. Study of biofilm growth on slippery liquid-infused porous surfaces made from fluoropor. *ACS applied materials & interfaces* **2019,** *11* (4), 4480-4487.
(71) Doll, K.; Fadeeva, E.; Schaeske, J.; Ehmke, T.; Winkel, A.; Heisterkamp, A.; Chichkov, B. N.; Stiesch, M.; Stumpp, N. S. Development of laser-structured liquid-infused titanium with strong biofilm-repellent properties. *ACS applied materials & interfaces* **2017,** *9* (11), 9359-9368.

For Table of Contents Use Only

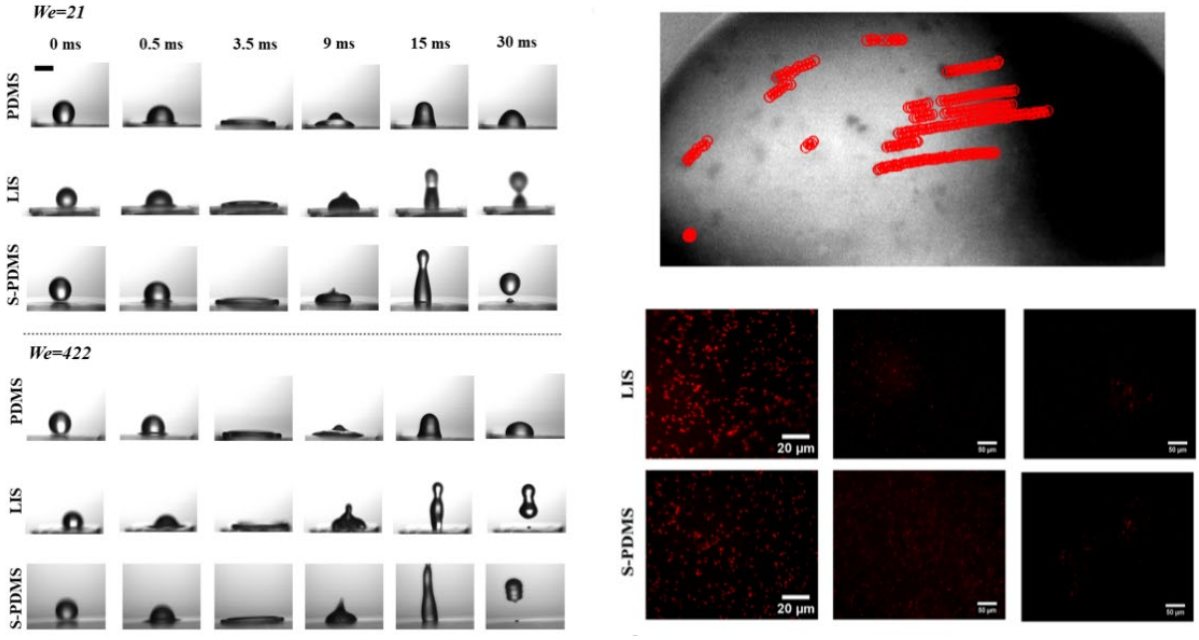

Supporting Information

Anti-wetting and anti-fouling performances of different lubricant-infused slippery surfaces

Yunyi Cao[†], Saikat Jana[†], Xiaolong Tan[ℓ], Leon Bowen[‡], Yufeng Zhu†, Jack Dawson†, Rui Han†, John Exton[†], Hongzhong Liu[§], Glen McHale[ǁ,#], Nicholas S. Jakubovics[⊥] and Jinju Chen[†]*

[†] School of Engineering, Newcastle University, Newcastle Upon Tyne, NE1 7RU, UK; [ℓ] School of Pharmacy, Newcastle University, Newcastle Upon Tyne, NE1 7RU, UK; [‡] Department of Physics, Durham University, Durham, DH1 3LE, UK;[§] School of Mechanical Engineering, Xi'an Jiaotong University, Xi'an 710054; [ǁ]Smart Materials and Surfaces Laboratory, Faculty of Engineering and Environment, Northumbria University, Newcastle upon Tyne, NE1 8ST, UK; [#]School of Engineering, University of Edinburgh, Edinburgh, EH9 3FB, UK; [⊥]School of Dental Sciences, Newcastle University, Newcastle Upon Tyne, NE2 4BW, UK.

Number of Pages: 5
Number of Figures: 5
Number of Tables: 1

Measurement of oil thickness for S-PDMS

We have now measured the weight (w1) of S-PDMS after a gentle wipe (the same protocol to prepare S-PDMS for the antifouling/antiwetting tests). Then, we measured the weight (w2) and the dimensions (x,y,z) of the swollen PDMS (after wiping off all surface oil).

In this case, we re-calculated the oil thickness (t) by assuming the oil layer thickness is uniformly in all directions. The following equation was used.

$$\frac{w1-w2}{oil\ density} = (x+2t)(y+2t)(z+2t) - xyz \quad \text{(S1)}$$

where x,y,z are the length, width and height of the swollen substrate.

Table S1. Calculations based on equations (1&2).”Epoxy” and “S.epoxy” indicate the epoxy nano-pillars without and with the surface salinization. Θ_{water} and Θ_{oil} are the average values from the measured static contact angles on flat substrates from at least three individual measurements. R represents the roughness factor of the substrate, which is the ratio between the actual and projected surface areas of the textured solids. In the case of epoxy nano-pillars, with width a (~1 μm), edge-to-edge spacing b (~2 μm), and height h (~2 μm), $R=1+\pi ah/(a+b)^2$. γ_{water}, γ_{oil} represent the surface tensions of water and silicone oil, taken from reference[1] and reference[2], respectively. γ_{ow} represents the interfacial tension for water- oil interface, taken from reference[2].

Solid	R	γ_{water}(mN/m)	γ_{oil}(mN/m)	γ_{ow} (mN/m)	Θ_{water}	Θ_{oil}	ΔE_1	ΔE_2	Stable
Epoxy	1.7	72.4	20.1	46.7	87	0	-18.97	80.03	no
S.Epoxy	1.7	72.4	20.1	46.7	120	60	31.99	130.99	yes

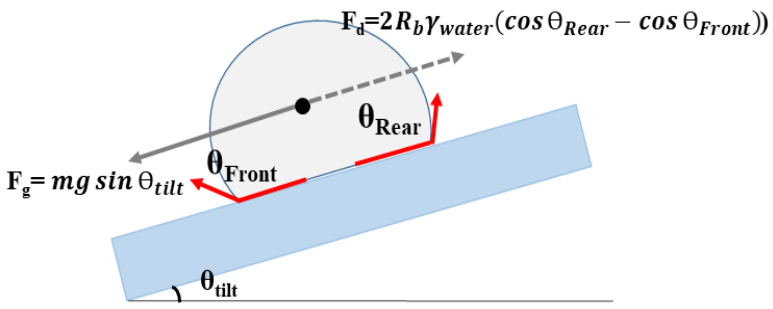

Figure S1. Schematic for the calculation of F_g and F_d as described in the main text.

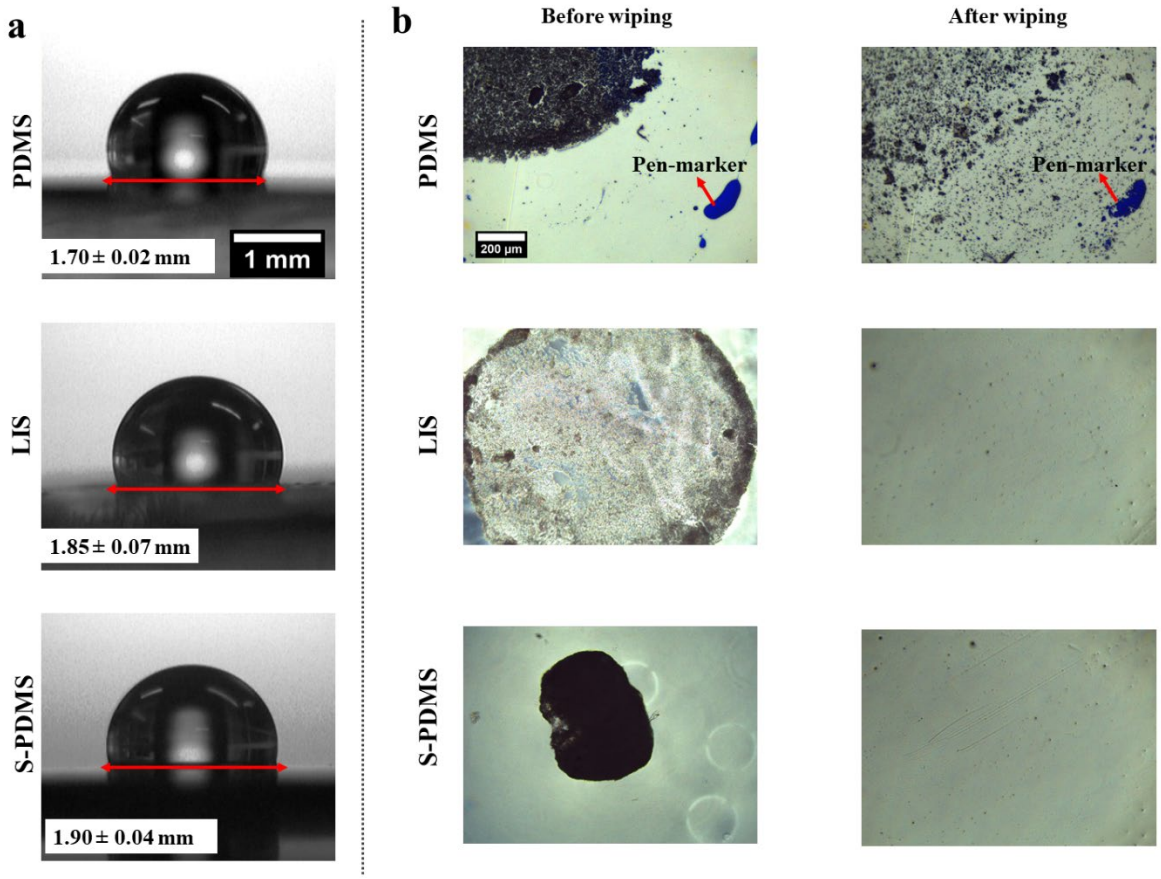

Figure S2. (a): The initial CL of 3 µl droplet of of a stardust aqueous solution on the surfaces of control PDMS, LIS and S-PDMS, respectively. (b): The dried stains on either LIS or S-PDMS can be easily removed by tissue papers, while the one on the PDMS collapsed into small particles and contaminated the whole surfaces.

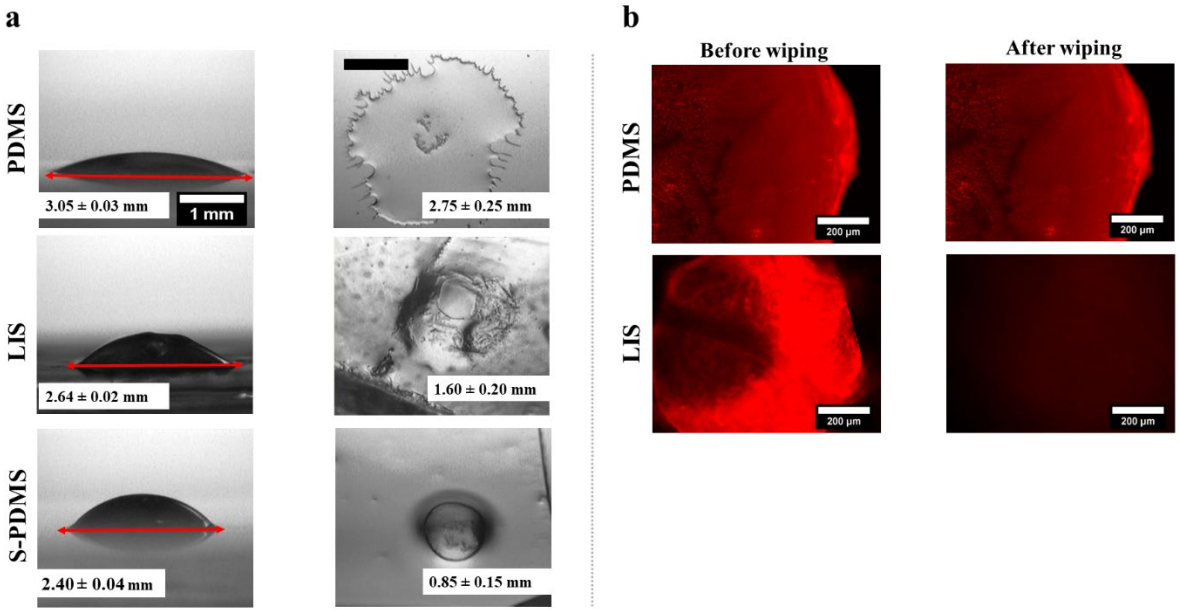

Figure S3. The evaporated biofilm droplet remained a coffee-ring-like stain on the PDMS surface, similar to the initial CL of biofilm culture droplet. The dried biofilm stain cannot be wiped or collapsed via the tissue papers, indicating its highly adhesion after drying on the PDMS surfaces. However, the biofilm stains on either LIS or S-PDMS were much smaller as compared to their initial biofilm droplet CLs, and the dried biofilm stains were still easily removed by tissue papers from either surface.Scale bar in (a) are all set as 1mm. Scale bar in (b) are all set as 200 μm.

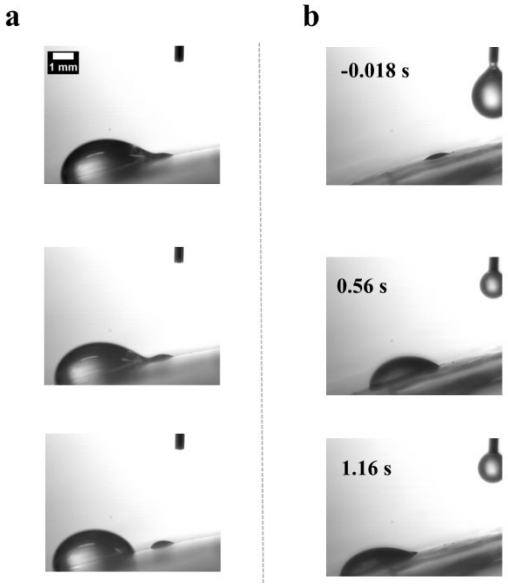

Figure S4. A 20 μl water droplet cannot peel away the stain on LIS easily with leaving water residues as shown in (a); however, the biofilm stains can still be peeled away after 2-3 times washing with a 20 μl water droplet as shown in (b).

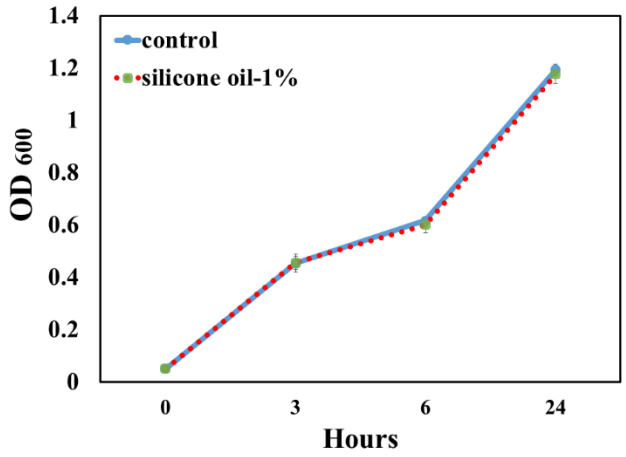

Figure S5. Indistinguishable growth curves of *P. aeruginosa* cultured in shaken TB media containing 1% of silicon oil at 0, 3, 6 and 24 h suggests no toxicity and biocompatibility of the lubricant.

1. Wong, T.-S.; Kang, S. H.; Tang, S. K.; Smythe, E. J.; Hatton, B. D.; Grinthal, A.; Aizenberg, J., Bioinspired self-repairing slippery surfaces with pressure-stable omniphobicity. *Nature* **2011,** *477* (7365), 443.
2. Smith, J. D.; Dhiman, R.; Anand, S.; Reza-Garduno, E.; Cohen, R. E.; McKinley, G. H.; Varanasi, K. K., Droplet mobility on lubricant-impregnated surfaces. *Soft Matter* **2013,** *9* (6), 1772-1780.